

OPEN ACCESS

On the kinematic structure of the Carina dwarf spheroidal galaxy

To cite this article: Michele Fabrizio *et al* 2012 *J. Phys.: Conf. Ser.* **383** 012009

View the [article online](#) for updates and enhancements.

You may also like

- [Integral Field Unit Observations of NGC 891: Kinematics of the Diffuse Ionized Gas Halo](#)
George H. Heald, Richard J. Rand, Robert A. Benjamin et al.
- [A Hubble Space Telescope WFPC2 Investigation of the Disk-Halo Interface in NGC 891](#)
Jörn Rossa, Ralf-Jürgen Dettmar, René A. M. Walterbos et al.
- [Characterization of PM10 accumulation periods in the Po valley by means of boundary layer profilers](#)
M E Ferrario, A Rossa and D Pernigotti



ECS
The
Electrochemical
Society
Advancing solid state &
electrochemical science & technology

DISCOVER
how sustainability
intersects with
electrochemistry & solid
state science research

On the kinematic structure of the Carina dwarf spheroidal galaxy

Michele Fabrizio¹, Ivan Ferraro², Giacinto Iannicola², Giuseppe Bono^{1,2}, Mario Nonino³ and Frédéric Thévenin⁴

¹Dept. Physics, Univ. Rome "Tor Vergata", Via della Ricerca Scientifica, 1 – 00133, Rome

²INAF–OAR, via Frascati 33, Monte Porzio Catone, Rome, Italy

³INAF–OAT, via G.B. Tiepolo 11, 40131 Trieste, Italy

⁴Univ. Nice Sophia-antipolis, CNRS, OCA, Lab. Lagrange, BP 4229, 06304 Nice, France

E-mail: michele.fabrizio@roma2.infn.it

Abstract. We present a semi-automatic interactive code, ROma Stellar Spectroscopic Analyzer (ROSSA), to measure radial velocities (RVs) from stellar spectra, covering a broad range of spectral resolutions. The measurement is supported by a graphical interface to change the fitting function (Gaussian or Moffat) and their parameters such as, e.g., symmetry and wings contribution. ROSSA has been applied to the kinematical structure of the Carina dwarf spheroidal galaxy, in order to obtain homogeneous RV measurements of ~ 1400 stars collected with various VLT spectrographs (FORS2, FLAMES/GIRAFFE medium- and high-resolution grisms). The spectroscopic targets cover different evolutionary phases and stellar populations of Carina, from the red giant branch to phases of old (horizontal branch) and intermediate age (red clump) helium burning stars. These stars are the tracers of two different star formation episodes (2-6 and 12 Gyr).

1. Introduction

Dwarf galaxies are fundamental laboratories to investigate the influence of the environment on star formation and chemical evolution in stellar systems that are several order of magnitudes smaller than giant galaxies. Empirical evidence indicates that in the Local Group (LG) together with the dwarf ellipticals (dE, M32-like) and the dwarf spirals (dS, M33-like) we are facing three different dwarf morphological types. The dwarf spheroidals (dSphs) show either single (Cetus, [15]; Tucana, [16]) or multiple star formation events (Carina, [2]), are spheroidal in morphology and lack of neutral hydrogen [3]. The dwarf irregulars (dIs) host a mix of old and young stellar populations, but they have recently experienced an intense star formation episode [17, 4], moreover, they have irregular morphology and host a significant fraction of gas and molecular clouds. The transition dwarfs have properties between the dSphs and the dIs. The observational scenario concerning the dwarfs in the LG was recently enriched by the discovery of ultra-faint dSphs in the SDSS [21, 18, 20], but their properties still need to be investigated in detail. Although the morphological classification appears robust, we still lack firm quantitative constraints concerning the evolution/transition between different dwarf morphological types. Kormendy et al. [12, 13] found a well defined difference between ellipticals (Es) and spheroidals [14]. Early type galaxies are distributed along a sequence moving from cD to dEs, while spheroidals are distributed along a sequence that overlaps with spirals and

dwarf irregulars (see Fig. 1 in [14]). This empirical dichotomy seems to suggest that E and Sph galaxies are stellar systems that underwent different formation and evolution processes. In particular, the Sphs might be either spirals or irregulars that lost their gas or transformed it into stars. However, there is no general consensus concerning the E–Sph dichotomy, since the correlation between the shape of the brightness profile and the galaxy luminosity is continuous when moving from Es to Sphs [9, 8, 7].

Precise and homogeneous photometric and spectroscopic data are required to address the above open issues concerning the formation and evolution of these systems. The advent of multi-object spectrographs at the 8-10m class telescopes provided the unique opportunity to collect sizable samples of low-, medium- and high-resolution spectra covering the entire body of nearby dwarf galaxies. By using tens of radial velocity (RV) measurements, it has been suggested by [11] that Sextans dSph hosts kinematic substructures, in particular, they found that the RV dispersion of the stellar population located across the center of this system is close to zero and increases outside the core. A different kinematic status has also been suggested by [1], using ~ 500 red giant (RG) stars, for the two distinct stellar populations in the Sculptor dSph.

In this context, Carina plays a key role because it is relatively close ($\mu=20.10$ mag), shows at least two well separated SF episodes ($t=2-6$ and 12 Gyr) and it is metal-poor ($\langle[\text{Fe}/\text{H}]\rangle\sim -1.7$ dex). In Fabrizio et al. [5] we provided RV measurements for ~ 1400 Carina candidate stars showing the occurrence of secondary kinematical feature across the center of the galaxy, suggesting a correlation with the transition properties detected in dwarf ellipticals [10]. The measurement of RVs was performed adopting an interactive code (ROSSA) described in the following.

2. ROma Stellar Spectroscopic Analyzer

The f77-code ROSSA is a semi-automatic software, with a graphical interface, meant to obtain accurate measurements of stellar radial velocities, independently from the evolutionary phase or metallicity of the star or the resolution of spectra.

To measure the RVs, we start measuring the peaks of well known spectral features. In particular, we selected strong spectral lines easily to recognize by eye inspection in observed spectra (e.g. $\text{H}\beta^1$, Mg I triplet², near infrared Ca I triplet³, Fe I⁴). All spectra are normalized to continuum, that is estimated with an iterative smoothing algorithm in order to avoid an over or underestimate across the strongest lines. The fitting of single or multiple blending lines is performed by using a Gaussian or a Moffat function. The user could fit each line by a Gaussian or by a Moffat function with different β values, to properly account the contribution of wings in the line fit. These peak positions give a preliminary estimation of RV and are weighted by the inverse of their amplitudes (a sharp line has more weight than a broad one). The preliminary estimate of the RV is validated by visual inspection and, when judged to be satisfactory, it was adopted to perform an automatic estimate of the RV.

The user must provide a line list with the reference wavelengths of several spectral lines (single or blended) that appear in the observed spectrum. Each line is fitted with a Moffat function ($\beta = 2$) that has a peak value, converted in RV, inside the spread of RV measured by hand in the previous step. The error in the RV based on individual lines was assumed to be equal to the sigma of the fitting function. In particular, we assume $\epsilon_{RV} = c\sigma_\lambda/\lambda$ km s⁻¹. Several checks are performed to discard spurious line identifications and fittings. In particular, are neglected lines with an amplitude smaller than half or greater than twice the line width given by the spectrograph resolution ($\sigma_\lambda = \lambda/R$). The RV of the entire spectrum was estimated as

¹ $\text{H}\beta$: $\lambda = 4861.34$ Å

² MgT: $\lambda = 5167.33, 5172.70, 5183.62$ Å

³ CaT: $\lambda = 8498.02, 8542.09, 8662.12$ Å

⁴ Fe I: $\lambda = 5429.70, 5434.53, 5446.92, 5455.62$ Å

a weighted mean over the different fitted lines (weights are chosen as the inverse of the errors). The error in the RV of the entire spectrum is the error of the weighted mean.

In Fig. 1 are shown two red giant stars (RG) of Carina dSph in a range of ≈ 2 mag. From top

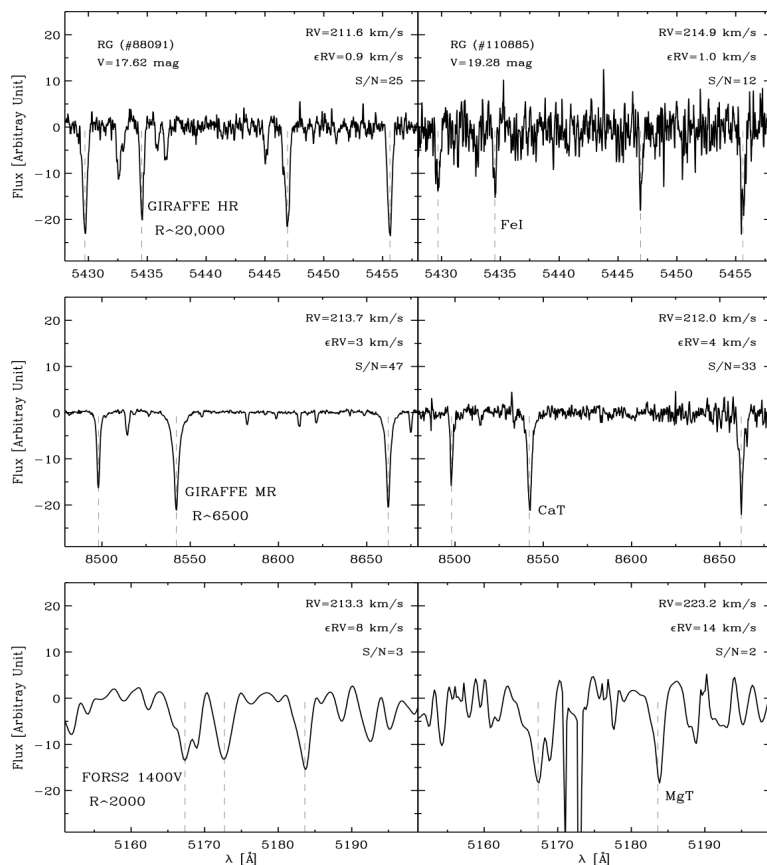


Figure 1. Left panels: from top to bottom are shown spectra of a Carina RG star with $V = 17.62$ mag, collected with three different spectrographs with decreasing spectral-resolution. Right panels: same as the left panels, but for a fainter Carina RG star with $V = 19.28$ mag.

to bottom panels, are shown the same stars observed with different spectrograph at ESO/VLT: FLAMES/GIRAFFE HR10 grism ($R \sim 20\,000$), FLAMES/GIRAFFE LR08 grism ($R \sim 6\,500$) and FORS2 1400V grism ($R \sim 2\,000$), respectively. Dotted lines display the spectral features adopted for the visual preliminary RV determination. The signal-to-noise ratios (S/N), RV values with their uncertainties are also labelled. All RVs agree, within the error, quite well. The uncertainties are bigger for spectra with lower S/N.

The power of this algorithm is the versatility across a broad range of spectrograph and stellar parameters. Indeed, the pros with respect to the most adopted method of the cross-correlation with a theoretical or empirical template, is the absolute independence from the stellar parameters. Therefore, it is possible to measure RV with high accuracy, for any metallicity, gravity and effective temperature. The only constraint is the visibility of spectral lines. The accuracy of the result, of course, will depend on the number of lines measured. Therefore, for example in an hot horizontal branch star ($T_{eff} \sim 20\,000$ K) will be measured just few broad lines, like $H\beta$ and He I, obtaining an accuracy smaller (~ 10 km s^{-1}) than one obtained with a red giant star with more than one hundred measured lines (~ 2 km s^{-1}).

Moreover, in order to improve the accuracy of the RV measurements, the user could choose

a modified Moffat function, based on two different β -values, to fit the asymmetric lines⁵ [19]. Fig. 2 shows an example of the asymmetric fit for one line of the Mg I triplet, at $\lambda = 5183.62 \text{ \AA}$, on a FORS2 low-resolution spectrum. This Mg I line, at the resolution of ~ 2000 , appears to be

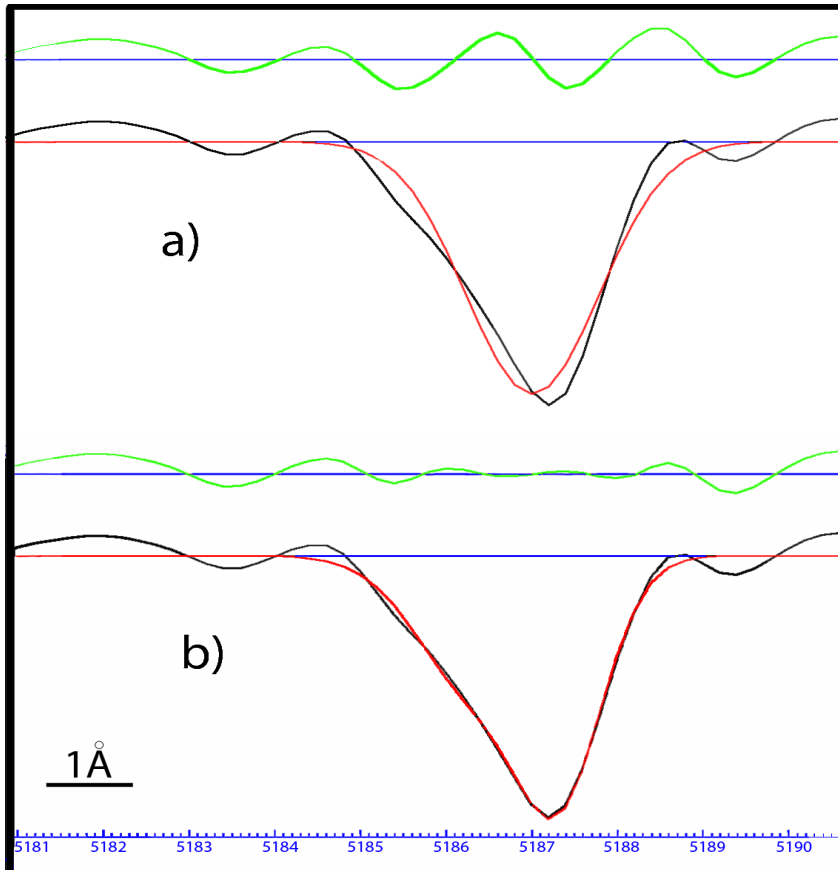


Figure 2. Fits with a Moffat function of the Mg I line on a low-resolution spectrum (not RV corrected) collected with FORS2@VLT (bottom right panel of Fig. 1). The fit showed in the top panel was performed by using a symmetric function, while the fit of the bottom panel was performed by adopting an asymmetric Moffat function with two different β -values. The red curves display the fit. The green curves are the residuals plot.

blended with the near absorption features (MgH, Fe I and Ni I), therefore shows a pronounced asymmetry. The green lines display the residuals of the fitting procedure, showing the better removal of the line wings (panel b) in both sides of the line respect to a symmetric fit with a Gaussian (panel a).

In order to simplify the measurement on the spectra, we introduced a list of possible options. For example, there is a complete list of options to produce a fit with fixed/variable peak or width or continuum level. A screenshot of the interactive software is shown in Fig. 3.

3. Conclusions

We developed a new software (ROSSA) to perform accurate radial velocity measurements from spectra covering a broad range of spectral resolutions. The main advantage of ROSSA, when compared with similar codes based on the cross-correlation technique, is that no theoretical or empirical grid of stellar templates is required. This means that ROSSA is particularly useful in dealing with large samples of stellar spectra collected with different spectrographs and covering a broad range of signal-to-noise ratios. At the same time, ROSSA can easily analyze spectra of stars in different evolutionary phases, and therefore covering a broad range of effective temperatures and surface gravities. We validated ROSSA by investigating the

⁵ The details of the modified Moffat fitting procedure will be described in a forthcoming paper, Ferraro et al. 2012.

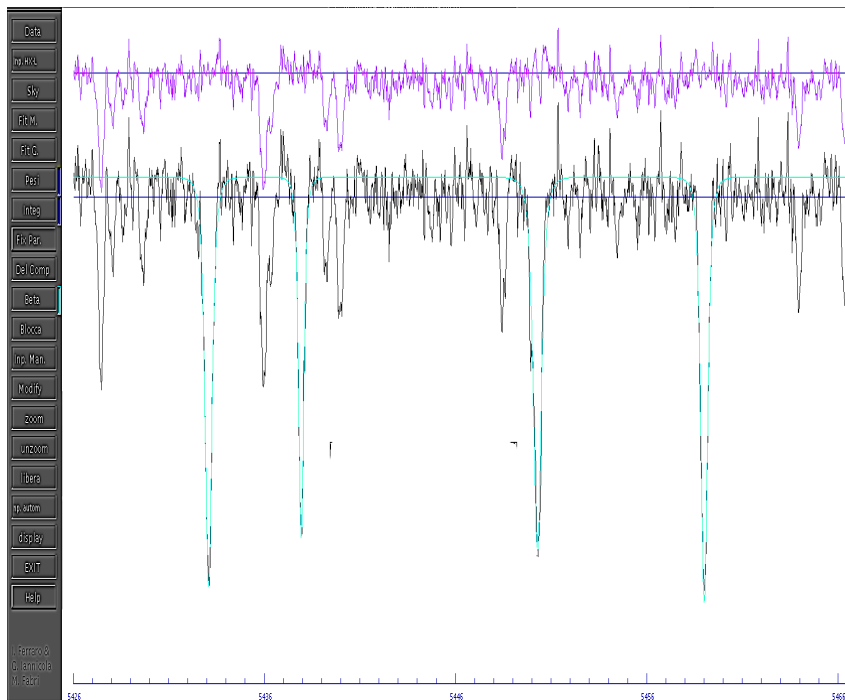


Figure 3. A screenshot taken from ROSSA on the FLAMES/GIRAFFE HR spectrum (top-right panel in Fig. 1). ROSSA was applied to four Fe I lines. On the left is visible a list of boxes listing the options that the user can use interactively to improve the quality of the fit. The color coding is the same as in Fig. 2.

kinematical structure of the Carina dSph. We used ~ 1400 spectra covering the entire body of the galaxy and we found evidence of substructure(s) across the central regions [5, 6].

Acknowledgments

MF would like to thank the organizers for the stimulating meeting. This work has been done in collaboration with the Carina project: M. Monelli, P. B. Stetson, A. R. Walker, P. François, R. Buonanno, F. Caputo, C. E. Corsi, M. Dall’Ora, R. Gilmozzi, C.R. James, T. Merle, L. Pulone and M. Romaniello.

References

- [1] Battaglia G., Helmi A., Tolstoy E., Irwin M., Hill V. and Jablonka P. 2008, *ApJ*, **681**, L13
- [2] Bono G., et al 2010, *PASP*, **122**, 651
- [3] Bouchard A., Jerjen H., Da Costa G.S. and Ott J. 2005, *AJ*, **130**, 2058
- [4] Cole A.A. 2010, *PASA*, **27**, 234
- [5] Fabrizio M., et al 2011, *PASP*, **123**, 384
- [6] Fabrizio M., 2011, PhD Thesis, Univ. Rome "Tor Vergata"
- [7] Ferrarese L., et al. 2006, *ApJS*, **164**, 334
- [8] Gavazzi G., Donati A., Cucciati O., Sabatini S., Boselli A., Davies J. and Zibetti S. 2005, *A&A*, **430**, 411
- [9] Jerjen H. and Bingeli B. 1997, in *ASP Conf. Ser.* **116**, The Second Stromlo Symposium: The Nature of Elliptical Galaxies (San Francisco: ASP), 239
- [10] Jerjen H., Kalnajs A. and Bingeli B. 2000, *A&A*, **358**, 845
- [11] Kleyra J.T., Wilkinson M.I., Evans N.W. and Gilmore, G. 2004, *MNRAS*, **354**, L66
- [12] Kormendy J. 1985, *ApJ*, **292**, L9
- [13] Kormendy J. 1987, in *IAU Symp.* **127**, Structure and Dynamics of Elliptical Galaxies (Cambridge: Cambridge Univ. Press), 17
- [14] Kormendy J., Fisher D.B., Cornell M.E. and Bender R. 2009, *ApJS*, **182**, 216
- [15] Monelli M., et al. 2010, *ApJ*, **720**, 1225
- [16] Monelli M., et al. 2010, *ApJ*, **722**, 1864
- [17] Sanna N., et al. 2009, *ApJ*, **699**, L84
- [18] Tolstoy E., Hill V., and Tosi M. 2009, *ARA&A*, **47**, 371
- [19] Wallerstein G., et al. 1992, *MNRAS*, **259**, 474

- [20] Wyse R.F.G. 2010, *AN*, **331**, 526
- [21] Zucker D.B., et al. 2006, *ApJ*, **650**, L41